Journal of Materials Chemistry B

ROYAL SOCIETY OF CHEMISTRY

PAPER

View Article Online
View Journal | View Issue



Check for updates

Cite this: *J. Mater. Chem. B*, 2023, **11**, 3979

# Tuning the 1D–2D dimensionality upon ligand exchange in silver thiolate coordination polymers with photoemission switching†

Saly Hawila,[a] Florian Massuyeau,[b] Romain Gautier,[b] Alexandra Fateeva,[c] Sébastien Lebègue,[d] Won June Kim,[e] Gilles Ledoux,[f] Adel Mesbah[a] and Aude Demessence*[a]

Received 14th March 2023,
Accepted 5th April 2023

DOI: 10.1039/d3tb00537b

rsc.li/materials-b

Silver nanoparticles are known and widely used for their antimicrobial activities. Nevertheless, once they are released into the natural or biological environments, they can become toxic with time, because of the dissolution of some Ag(I) ions that can then react with thiol-based molecules, such as glutathione and/or compete with copper proteins. These assumptions are based on the high affinity of the soft acid Ag(I) and the soft base thiolates and the exchange reactions that are involved in complex physiological media. Here we synthesized and fully characterized two new 2D silver thiolate coordination polymers (CPs) that exhibit a reversible 2D-to-1D structural transformation in the presence of an excess of thiol molecules. This dimensionality change induces also a switch of the yellow emission of the Ag-thiolate CP. This study highlights that these highly stable silver-thiolate CPs, in basic, acidic and oxidant media can undergo a complete dissolution–recrystallization mechanism upon thiol exchange reactions.

## Introduction

In our daily life, silver nanoparticles are widely used as biocides, for their antimicrobial activity, in textiles, food packaging, drinking water and medical devices such as pads or catheters.[1] Their biocidal activity is due to the high toxicity of Ag(I) ions that are released from silver nanoparticles.[2] Thus, during their life cycle, silver nanoparticles, and more particularly Ag(I) soluble species, are dispersed in the environment where they are subjected to various reactions throughout the cells in bacteria, plants or animals with different toxic potential. Ag(I) is an unphysiological ion, and it displays similar soft acid character to the physiological Cu(I) and comparably high binding affinity for thiolate ligands that are soft bases. Thiol-based molecules present in cells are mainly glutathione and metallothionein, which are important proteins involved in cellular copper homeostasis. Consequently, it has been proposed that the toxicity of Ag(I) ions in cells is due to their ability to easily bind to thiol biomolecules and replace Cu(I) in their native binding sites that are involved in Cu(II)/Cu(I) redox reactions.[3] This copper to silver replacement prevents the redox reactions that involve the Cu(II)/Cu(I) couple. Nevertheless, the nature of the Ag(I)–thiolate complexes formed within cells is poorly understood, and the details of Ag(I) coordination in such complexes are mostly unknown. Fast exchange reactions in silver thiolates have been investigated, and have been proposed to be the mechanism of transfer of silver to biota, but no in depth studies supporting this propasal have been reported.[4]

In order to design the best functionalized silver nanoparticles as antimicrobial agents and avoid the toxicity of Ag(I) ions, it is crucial to understand the chemistry of Ag(I) and thiolates in terms of structure, stability and reactivity.[5] From a structural point of view, neutral $[Ag(SR)]_n$ compounds are reported as cyclic oligomers with bulky thiolate ligands,[6] or as 1D coordination polymers (CPs):[7] $[Ag(o\text{-}SPhCO_2X)]_n$ X = H[8] and Me,[9] or as 2D CPs: $[AgSPh]_n$,[10] $[Ag(p\text{-}SPhCO_2X]_n$ X = H and Me.[11] Some of these CPs have shown antimicrobial activities.[12]

[a] Université Lyon, Université Claude Bernard Lyon 1, Institut de Recherches sur la Catalyse et l'Environnement de Lyon (IRCELYON), UMR CNRS 5256, Villeurbanne, France. E-mail: aude.demessence@ircelyon.univ-lyon1.fr
[b] Nantes Université, CNRS, Institut des Matériaux de Nantes Jean Rouxel, IMN, Nantes F-44000, France
[c] Université Lyon, Université Claude Bernard Lyon 1, Laboratoire des Multimatériaux et Interfaces (LMI), UMR CNRS 5615, Villeurbanne, France
[d] Université de Lorraine, Laboratoire de Physique et Chimie Théoriques (LPCT), UMR CNRS 7019, Vandœuvre-lès-Nancy, France
[e] Changwon National University, Department of Biology and Chemistry, Gyeongsangnam-do, South Korea
[f] Université Lyon, Université Claude Bernard Lyon 1, Institut Lumière Matière (ILM), UMR CNRS 5306, Villeurbanne, France

† Electronic supplementary information (ESI) available: Characterization techniques, syntheses, and SEM, TGA, PXRD, SHG, FT-IR, UV-visible and photoluminescence results. CCDC 2245604 and 2245602. For ESI and crystallographic data in CIF or other electronic format see DOI: https://doi.org/10.1039/d3tb00537b

In this study we focused on the chemical stability of Ag(I)-thiolate compounds and more importantly their ability to display thiolate ligand exchanges, which may facilitate Ag(I) to enter in a cell. Indeed, full thiolate ligand and silver isotope exchanges have been reported for atomically defined silver thiolate clusters and the metallic core remained the same during the processes.[13] In addition, some insoluble fluorinated silver-thiolate derivatives were able to react with bis(diphenylphosphane)methane and dichloromethane, pointing out the capability of silver thiolate to cleave C–Cl bonds.[14] Some insoluble silver thiolate CPs were also used as precursors for the synthesis of silver thiolate clusters, pointing out the reactivity of these CPs.[15]

Here the synthesis and structure of two new 2D silver thiolate materials are presented: $[Ag(p\text{-SPhF})]_n$ (**1**) and $[Ag(p\text{-SPhCl})]_n$ (**2**) and the studies of their stability in basic, acidic, reducing and oxidative media are presented. More importantly, this paper shows that in the presence of an excess of thiol, these 2D CPs are dissolved and recrystallize in a 1D network that exhibits an intense yellow photoemission.

## Results and discussion

### Syntheses and characterization

The formation of $[Ag(p\text{-SPhF})]_n$ (**1**) and $[Ag(p\text{-SPhCl})]_n$ (**2**) proceeds through a reaction between $AgNO_3$ and the corresponding thiol ligand in water and a mixture of water/methanol, respectively, for 2 h at room temperature (RT) (see the ESI†). The powder X-ray diffraction (PXRD) patterns of **1** and **2** show predominant *00ℓ* reflections characteristic of lamellar structures with interlamellar distances of 14.7 and 16.3 Å, respectively (Fig. 1). These distances correspond well to two layers of silver-ligand without interpenetration of the molecules. The SEM images of **1** and **2** show that these compounds are composed of quite homogenous crystallites of a few hundred nanometer diameters (around 340 nm and 140 nm, respectively) (Fig. S1, ESI†). The thermogravimetric analyses confirm the neutral chemical composition of $[Ag(SR)]_n$ and purity of **1** and **2** with a remaining of silver content corresponding to the expected values: 46.7% (calculated: 45.9%) for **1** and 42.1% (calculated: 42.8%) for **2** (Fig. S2, ESI†). In addition, the TGA curves show a relatively good thermal stability of both CPs of up to 200 °C in air. The C, H, and S elemental analyses also support the metal/ligand ratio = 1 (see the ESI†).

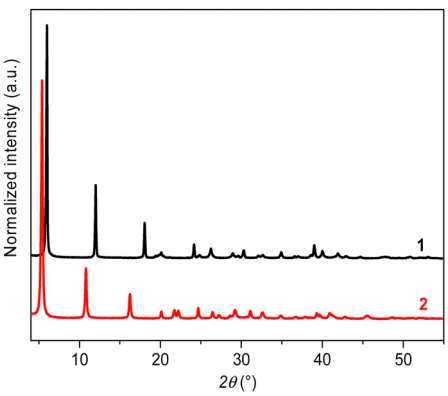


Fig. 1 PXRD patterns of the as synthesized 2D **1** and **2** CPs.

### Structure description

The powder X-ray diffraction (PXRD) data, collected at the CRISTAL beamline of the SOLEIL synchrotron facility, show good crystallinity and allow *ab initio* structural determinations. The final Rietveld refinements of **1** and **2** (Fig. S3 and S4, ESI†) lead to satisfactory model indicators and profile factors (Table S1, ESI†). $[Ag(p\text{-SPhF})]_n$ (**1**) crystallizes in the monoclinic $P2_1/n$ space group. The unit cell parameters are $a$ = 4.6917(1) Å, $b$ = 29.3556(6) Å, $c$ = 4.6950(1) Å and $\beta$ = 100.53 (1)°, including four formula units per cell. However, $[Ag(p\text{-SPhCl})]_n$ (**2**) crystallizes in the orthorhombic system in the *Iba*2 space group with $a$ = 32.5519(12) Å, $b$ = 7.3734(2) Å, $c$ = 5.8211(1) Å and eight formula units per cell. In each compound, the asymmetric unit is composed of one Ag atom and one *p*-SPhX molecule with X = F, Cl. In **1**, and each Ag atom is connected to four sulfur atoms with Ag-S interatomic distances ranged between 2.56(3) Å and 2.68(2) Å (Fig. 2a and Table S2, ESI†). In **2**, each Ag atom is connected to three sulfur atoms with Ag–S distances comprising between 2.296(9) Å and 2.722(11) Å (Fig. 2d and Table S2, ESI†). A fourth sulfur could be found at a distance of 3.092(1) Å, which is too long to be considered as a coordinating bond. The grid pattern of $\{AgS\}_n$ in **1** is similar to the one in $[Ag(SPh)]_n$ 2D CP[10] and the $\{AgS\}_n$ honeycomb network of **2** has been observed in $[Ag(p\text{-SPhCO}_2H/Me)]_n$ 2D CPs.[11] The central projection views of the inorganic layers and the overall structures are viewed in Fig. 2b and e. Both structures consist of infinite Ag–S inorganic layers separated by non-interpenetrated organic molecules. The main difference between the two structures is related to the presence of weak halogen interactions in **1** and their absence in **2**, inducing different crystal packings. Indeed in **1**, the organic layers are alternated while in **2** they face each other. Thus, **1** displays C–F···F–C interactions with an F···F distance of 2.965(2) Å. These interactions are of type I (parallel displaced geometry),[16] where $\theta_1 = \theta_2$ = 109.55(7)° (Fig. 2c and Fig. S5, ESI†). The C–H···F–C and C–F···π interactions are of 2.647(5) Å and 3.391(5) Å, respectively (Table S3, ESI†). In **2**, the Cl···Cl distance is 3.790(9) Å, which is at the limit of the double of the van der Waals radius of the chlorine atom, which varies from 1.74 to 1.9 Å,[17] to be considered as halogen interactions (Fig. 2f).

### Spectroscopic studies

As **2** crystallizes in the non-centrosymmetric *Iba*2 space group, its non-linear optical effect, such as the Second Harmonic Generation (SHG), has been evaluated.[18] Indeed, it displays a SHG signal at 400 nm under a 800 nm wavelength laser excitation at RT (Fig. S6, ESI†). When compared to the KDP (Potassium Dihydrogen Phosphate used as a reference) signal, the SHG signal intensity remains modest, as it has been observed for other Ag(I) CPs.[19]

The FT-IR spectra of **1** and **2** show the absence of the peak of the –SH stretching frequency around 2600–2550 $cm^{-1}$, which confirms the total deprotonation of the thiol groups and the

 

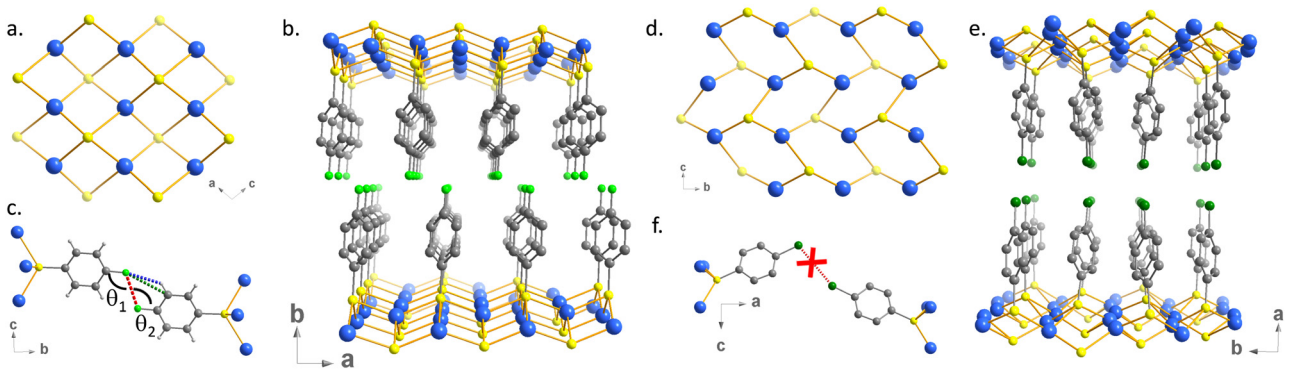


Fig. 2 Crystallographic structures of **1** and **2**, (a) representation of the $\{AgS\}_n$ network of **1** in the (a–c) plane, (b) central projection of the lamellar structure of **1**, (c) representation of the halogen interactions in **1**, the red dotted line is for F···F = 2.965(2) Å, the green dotted line for F···C = 3.391(5) Å and the blue dotted line for F···H = 2.647(5) Å, (d) representation of the $\{AgS\}_n$ network of **2** on the (b–c) plane, (e) central projection of the lamellar structure of **2** and (f) view of the absence of halogen interaction in **2**. Blue spheres are for, Ag(I); yellow, S; light green, F; dark green, Cl and grey, C. Most hydrogen atoms are omitted for clarity.

coordination of the thiolates to Ag(I) (Fig. S7, ESI†). Then, DFT simulations have been carried out to calculate the IR spectra of the compounds and assign the vibrational bands (Fig. 3 and Table 1). The calculated FT-IR spectra of **1** and **2** reproduce well the experimental ones. Nevertheless, while the symmetric vibration $\nu_s$ (C═C) of **1** is observed at 1593 $cm^{-1}$ and calculated at 1588 $cm^{-1}$, for **2** the band is calculated at 1562 $cm^{-1}$, and this vibration, which is not clearly seen, might be present in the noise. This may be related to the different electronegativity of the halogens.[20] Still the antisymmetric vibrations $\nu_{as}$ (C═C) of both compounds are correctly observed and calculated around 1380 and 1490 $cm^{-1}$, pointing out the presence of these aromatic carbons. In addition, shifts of $\nu$ (C–X) and $\nu$ (C–S) to the lower wavenumbers are observed from **1** to **2**; this may be related to the different electronegativity of the halogens and the different coordination modes of the thiolates to the silver atoms.

The solid-state UV-visible absorption spectra show that the two compounds exhibit high-energy absorption, with a maximum at 386 and 350 nm for **1** and **2**, respectively (Fig. S8, ESI†). This absorption can be assigned to π–π* transitions of the phenyl groups,[13] or to the metal-perturbed intra-ligand or ligand-to-metal charge-transfer transitions.[14] The estimated optical band gaps from these data are around 2.9 eV for **1** and **2**. These values are in the range of the calculated ones: 3.1 eV for **1** and 3.9 eV for **2**. The two compounds under UV light and temperatures from 20 °C to −180 °C are not emissive in the yellow to near infrared range (Fig. S9, ESI†). Non-luminescent 2D silver-thiolate CPs have been already reported, such as $[Ag(p\text{-}SPhCO_2X]_n$ (X = H and Me).[11]

## Chemical, thermal and mechanical stabilities

The chemical, thermal and mechanical stabilities in different media of **1** and **2** are studied (Fig. 4 and Fig. S10 and details of the experimental conditions are shown in the ESI†). In Fig. 4, it can be seen that **1** retains its crystallinity upon hand grinding for 30 min. **1** is also stable when heated in the solid state at 200 °C for 1 h in air and dispersed in water in a closed vial heated at 120 °C for 24 h. Then, **1** retains its crystallinity without any decomposition under basic conditions (NaOH 1 M, 120 °C, 24 h), acidic medium ($H_2SO_4$ 1 M, 120 °C, 24 h) and an oxidant environment ($H_2O_2$ 0.01 M, RT, 48 h) (Fig. 4). Nevertheless, when **1** is dispersed in a reducing medium ($LiBH_4$ 2 M, RT, 30 min), it completely decomposes and Ag(I) is reduced into bulk silver, as it can be observed by PXRD (Fig. 4). Compound **2** exhibits the same behavior under the same conditions (Fig. S10, ESI†). These tests

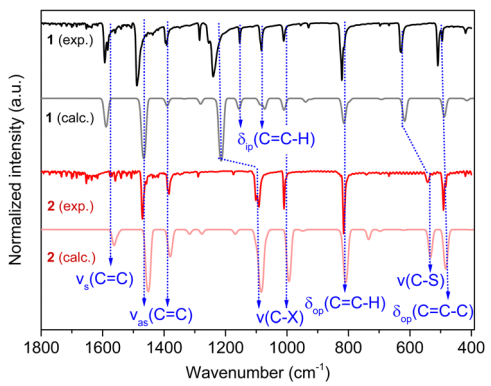


Fig. 3 Experimental and calculated FT-IR spectra of **1** and **2** and the assignments of the bands.

Table 1 Vibrational spectral assignments of **1** and **2**

| | FTIR frequency ($cm^{-1}$) of **1** | | FTIR frequency ($cm^{-1}$) of **2** | |
|---|---|---|---|---|
| Band assignment | Observed | Calculated | Observed | Calculated |
| $\nu_s$ (C═C) | 1593 | 1588 | — | 1562 |
| $\nu_{as}$ (C═C) | 1393 | 1390 | 1383 | 1379 |
| | 1488 | 1465 | 1470 | 1451 |
| $\nu$ (C–X) | 1010 | 1009 | 1009 | 993 |
| | 1240 | 1214 | 1096 | 1083 |
| $\delta_{ip}$ (C═C–H) | 1083 | 1080 | — | — |
| | 1153 | 1156 | | |
| $\delta_{op}$ (C═C–H) | 821 | 814 | 815 | 808 |
| $\nu$ (C–S) | 629 | 617 | 542 | 533 |
| $\delta_{op}$ (C═C–C) | 509 | 488 | 490 | 483 |

$\nu_s$: symmetric vibration, $\nu_{as}$: antisymmetric vibration, $\delta_{ip}$: in-plane bending, and $\delta_{op}$: out-of-plane bending.

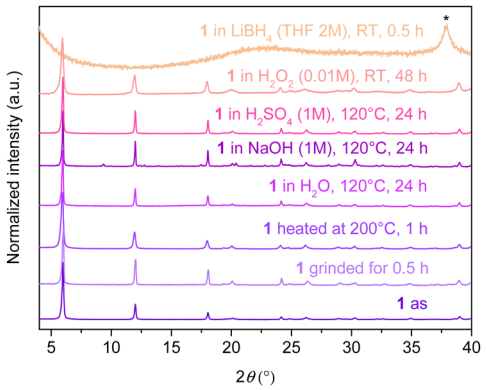


Fig. 4 PXRD patterns of **1** as-synthesized (as) and treated under grinding, heated at 200 °C under air and dispersed in water, basic, acidic, oxidant and reducing media. The black star is for bulk silver reflection.

confirm the high thermal stability and chemical robustness of these compounds in basic, acidic and oxidizing media, which is generally the case of silver(I)[21] and copper(I)[22] CPs that are based on the strong soft base and soft acid interactions.

### Exchange reactions

In order to study the behaviour of silver-thiolate CPs in the presence of excess of thiol molecules, **1** and **2** were dispersed, independently, in methanol and methyl thiosalicylate (*o*-$HSPhCO_2Me$) was added in excess. Then the vial was sealed and heated at 120 °C for different times. The choice of methyl thiosalicylate as the thiol molecule is based on its reactivity with Ag(I) to form $[Ag(o\text{-}SPhCO_2Me)]_n$ (**3**),[9] that is a 1D CP (Fig. 5a) characterized by a PXRD pattern completely different from the 2D **1** and **2** CPs. In addition, **3** is a yellow powder that exhibits intense yellow emission under UV light at RT, contrary to **1** and **2**, which are white and non-emissive powders (Fig. 5b and c).

From the PXRD patterns, the reaction of **1** with an excess of *o*-$HSPhCO_2Me$ for 18 h at 120 °C leads to a mixture of **1** and $[Ag(o\text{-}SPhCO_2Me)]_n$ ($\mathbf{3'_{(1)}}$), suggesting that the exchange is only partial. The addition of more methyl thiosalicylate to this mixture and an additional 18 h reaction at 120 °C, allow the synthesis of $\mathbf{3_{(1)}}$ with a PXRD diagram that corresponds to the simulated 1D $[Ag(o\text{-}SPhCO_2Me)]_n$ CP (Fig. 5d). The ligand exchange from **2** with an excess of *o*-$HSPhCO_2Me$ was proceeded for 48 h at 120 °C and the 1D phase of $\mathbf{3_{(2)}}$ was observed on the PXRD (Fig. S11, ESI†). The complete ligand exchange and purity of $\mathbf{3_{(1)}}$ and $\mathbf{3_{(2)}}$ were also confirmed by FT-IR, showing two similar spectra and the appearance of the vibrations of the carbonyl bands of the ester at 1705 $cm^{-1}$ (Fig. S12, ESI†). The TGA experiments provide a remaining silver content of 40.6 and 40.0% for $\mathbf{3_{(1)}}$ and $\mathbf{3_{(2)}}$, respectively, close to the expected calculated value of 39.2% for $[Ag(o\text{-}SPhCO_2Me)]_n$ CP (**3**) (Fig. S13, ESI†). The SEM images of these phases show needle crystallites of few hundred nanometer diameters and few micrometer lengths, typical of the 1D structure of **3** (Fig. 5e). In addition, unlike the lamellar **1** and **2**, which are

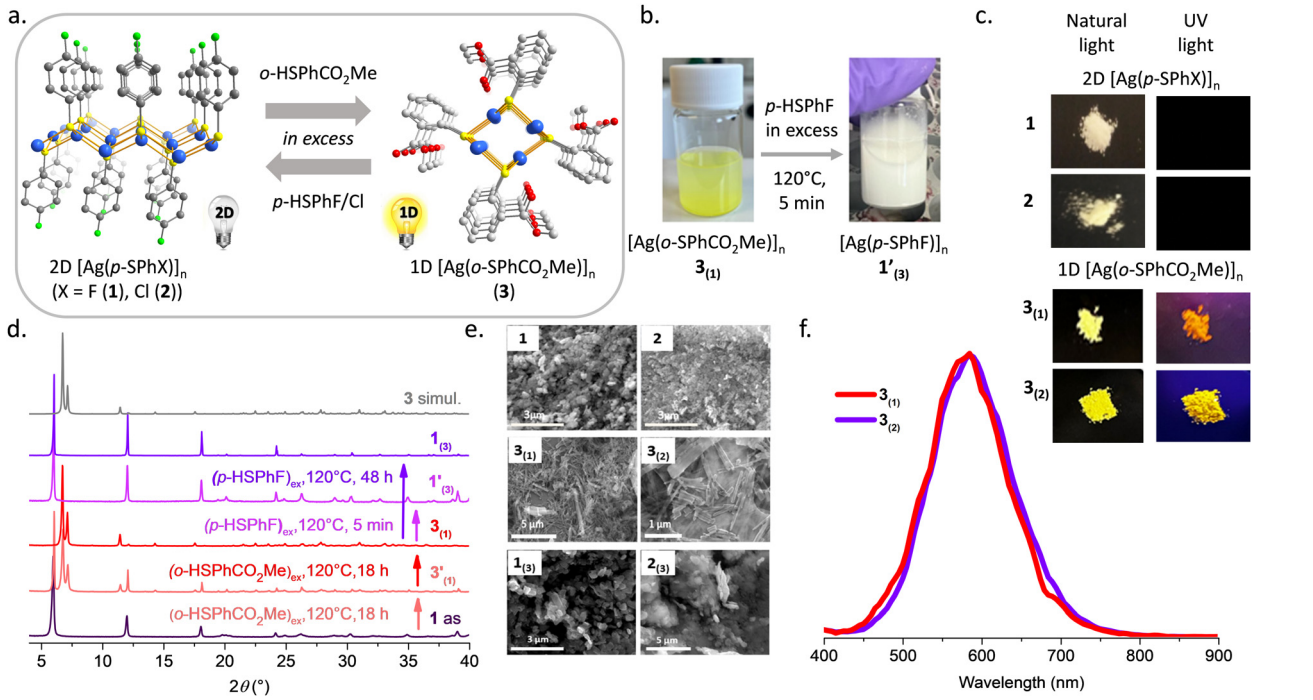


Fig. 5 Ligand exchange reactions in silver thiolate CPs. (a) Scheme of the ligand exchange between the 2D $[Ag(p\text{-}SPhX)]_n$ (X = F and Cl) and 1D $[Ag(o\text{-}SPhCO_2Me)]_n$; (b) photos of the yellow suspension of $\mathbf{3_{(1)}}$ and the white one of $\mathbf{1'_{(3)}}$; (c) photos under natural (left) and UV (right) lights of the **1** and **2** as synthesized and $\mathbf{3_{(1)}}$ and $\mathbf{3_{(2)}}$ obtained after ligand exchange reactions; (d) PXRD patterns of **1** as synthesized, $\mathbf{3'_{(1)}}$, $\mathbf{3_{(1)}}$, $\mathbf{1'_{(3)}}$ and $\mathbf{1_{(3)}}$ obtained after ligand exchange reactions and the simulated diagram of **3**; (e) SEM images of **1**, **2**, $\mathbf{3_{(1)}}$, $\mathbf{3_{(2)}}$, $\mathbf{1_{(3)}}$ and $\mathbf{2_{(3)}}$ and (f) solid state emission spectra of $\mathbf{3_{(1)}}$ and $\mathbf{3_{(2)}}$ at RT ($\lambda_{ex}$ = 320 nm).

 

non-luminescent, the 1D $\mathbf{3}_{(1)}$ and $\mathbf{3}_{(2)}$ exhibit yellow emission centred at 585 nm in the solid state and at RT (Fig. 5c and f and Fig. S14, ESI†). The light emission of **3** originates from a Ligand-to-Metal Charge Transfer (LMCT).[9] These ligand exchange reactions clearly show that the 2D-to-1D structure transformation accompanied by a switch on of the photoluminescence is only possible through a dissolution–recrystallization mechanism. To the best of our knowledge, this is the first study involving phase changes upon ligand exchange in neutral and highly stable Ag(I)-thiolate CPs. A report on a positively charged nitrogen-based Ag(I) CP shows its structural variation from 1D to 2D upon heating in solution.[19a] Nevertheless the reversibility of the phase change was not reported.

Here, the inverse ligand exchange reactions from **3** to **1** and **2** were performed. Thus, when the 1D $\mathbf{3}_{(1)}$ and $\mathbf{3}_{(2)}$ were dispersed in an excess of *p*-HSPhX (X = F, Cl) in methanol at 120 °C, the 2D $[Ag(p\text{-SPhX})]_n$ phases, $\mathbf{1}_{(3)}$ and $\mathbf{2}_{(3)}$, were obtained (Fig. 5d and Fig. S11, ESI†). The kinetics for these exchange reactions are much faster than for the previous ones; in 5 min a color change from yellow to white is observed (Fig. 5b) and the PXRD of $\mathbf{1}'_{(3)}$ matches the 2D $[Ag(p\text{-SPhF})]_n$ phase. Increasing the time reaction of 48 h allow to increase the crystallinity of $\mathbf{1}_{(3)}$ (Fig. 5d). Complete ligand exchange reactions from $\mathbf{3}_{(2)}$ to $\mathbf{2}_{(3)}$ can be completed in 1 h (Fig. S11 and S15, ESI†). The SEM images of $\mathbf{1}_{(3)}$ and $\mathbf{2}_{(3)}$ show that these compounds are composed of particles of a few hundred nanometer diameters (around 470 nm and 860 nm, respectively). Note that these crystallites are bigger than **1** and **2** compounds obtained by direct syntheses, due to the different crystallization mechanisms involved (Fig. 5e).

Finally, when silver-thiolate CPs are present along with an excess of thiol molecules, they undergo ligand exchange reactions implying a dissolution–recrystallization mechanism that allow in this study to go from non-luminescent 2D $[Ag(SR)]_n$ CPs to yellow emissive 1D compounds. This reversible 1D-to-2D phase changes prove that silver-thiolate structures are ligand dependent like gold thiolate CPs.[23]

## Conclusions

Two new 2D silver halogen-based thiolate CPs, $[Ag(p\text{-SPhF})]_n$ (**1**) and $[Ag(p\text{-SPhCl})]_n$ (**2**), have been reported. Thanks to the strong affinity between thiolate and Ag(I), these CPs show good stability at temperature up to 200 °C under air and under acidic, basic and oxidising conditions, but they decompose in a reducing medium. Moreover, they undergo 2D-to-1D transformation in the presence of an excess of methyl thiosalicylate implying a dissolution–recrystallization mechanism and so allowing to convert from non-luminescent 2D compounds to a luminescent 1D CP. This study highlights the high potential of silver thiolate for ligand exchange, and shows that the structure is dependent on the ligand and does not involve any topotactic structural changes, as it has been observed for some silver thiolate clusters.[13] This reversible 2D-to-1D transformations show that unphysiological silver ions can easily enter the biological cells by thiol exchange reactions with the main proteins, involving many diseases. Further experimental studies have to be carefully carried out to understand in-depth the reactivity of silver-thiolate compounds in natural and physiological environments, meaning in the presence of excess of thiol-based proteins and Cu(I)-based metalloproteins. This knowledge of silver-thiolate reactivity and stability will allow developing new biocompatible and antimicrobial silver nanoparticles without any side effects of Ag(I) toxicity in biological media.

## Author contributions

SH performed all the synthetic experiments and routine characterization; FM and RG carried out and interpreted the SHG experiments; AF took the SEM images, SL and WJK performed the DFT calculations; GL brought his photoluminescence apparatus and expertise; AM solved the crystal structures; AM and AD supervised and SH and AD wrote the manuscript. All authors revised the paper.

## Conflicts of interest

There are no conflicts to declare.

## Acknowledgements

The authors acknowledge SOLEIL synchrotron (Gif-sur-Yvette, France) for provision of radiation facilities (BAG for X-ray diffraction 20201440) and Erik Elkaïm for assistance in using CRISTAL beamline, the Centre Technologique des Microstructures of the University of Lyon for providing the electron microscopy facilities. This work was supported by the French National Agency (MOTIC ANR-21-CE08-0045). SH acknowledges the CNRS for her PhD grant. The European Commission is acknowledged by AD for her Marie Skłodowska-Curie Individual Fellowship (101031503—AniMOC—H2020-MSCA-IF-2020). W. J. K. and S. L. acknowledge financial support from the French-Korean program STAR.

## Notes and references

1 (*a*) M. Bosetti, A. Massè, E. Tobin and M. Cannas, *Biomaterials*, 2002, **23**, 887; (*b*) K. Chaloupka, Y. Malam and A. M. Seifalian, *Trends Biotechnol.*, 2010, **28**, 580; (*c*) K. M. Fromm, *Nat. Chem.*, 2011, **3**, 178; (*d*) K. Mijnendonckx, N. Leys, J. Mahillon, S. Silver and R. Van Houdt, *BioMetals*, 2013, **26**, 609.

2 (*a*) A. Ivask, A. ElBadawy, C. Kaweeteerawat, D. Boren, H. Fischer, Z. Ji, C. H. Chang, R. Liu, T. Tolaymat, D. Telesca, J. I. Zink, Y. Cohen, P. A. Holden and H. A. Godwin, *ACS Nano*, 2014, **8**, 374; (*b*) S.-L. Abram and K. M. Fromm, *Chem. – Eur. J.*, 2020, **26**, 10948.

3 G. Veronesi, T. Gallon, A. Deniaud, B. Boff, C. Gateau, C. Lebrun, C. Vidaud, F. Rollin-Genetet, M. Carrière, I. Kieffer, E. Mintz, P. Delangle and I. Michaud-Soret, *Inorg. Chem.*, 2015, **54**, 11688.

4 R. A. Bell and J. R. Kramer, *Environ. Toxicol. Chem.*, 1999, **18**, 9.
5 M. Marchioni, G. Veronesi, I. Worms, W. L. Ling, T. Gallon, D. Leonard, C. Gateau, M. Chevallet, P.-H. Jouneau, L. Carlini, C. Battocchio, P. Delangle, I. Michaud-Soret and A. Deniaud, *Nanoscale Horiz.*, 2020, **5**, 507.
6 O. Veselska and A. Demessence, *Coord. Chem. Rev.*, 2018, **355**, 240.
7 Q. Wang, S.-L. Dong, D.-D. Tao, Z. Li and Y.-B. Jiang, *Coord. Chem. Rev.*, 2021, **432**, 213717.
8 O. Veselska, N. Guillou, M. Diaz-Lopez, P. Bordet, G. Ledoux, S. Lebègue, A. Mesbah, A. Fateeva and A. Demessence, *ChemPhotoChem*, 2022, **6**, e202200030.
9 A. Abdallah, S. Vaidya, S. Hawila, S.-L. Ornis, G. Nebois, A. Barnet, N. Guillou, A. Fateeva, A. Mesbah, G. Ledoux, A. Bérut, L. Vanel and A. Demessence, *iScience*, 2023, **26**, 106016.
10 E. A. Schriber, D. W. Paley, R. Bolotovsky, D. J. Rosenberg, R. G. Sierra, A. Aquila, D. Mendez, F. Poitevin, J. P. Blaschke, A. Bhowmick, R. P. Kelly, M. Hunter, B. Hayes, D. C. Popple, M. Yeung, C. Pareja-Rivera, S. Lisova, K. Tono, M. Sugahara, S. Owada, T. Kuykendall, K. Yao, P. J. Schuck, D. Solis-Ibarra, N. K. Sauter, A. S. Brewster and J. N. Hohman, *Nature*, 2022, **601**, 360.
11 O. Veselska, C. Dessal, S. Melizi, N. Guillou, D. Podbevšek, G. Ledoux, E. Elkaim, A. Fateeva and A. Demessence, *Inorg. Chem.*, 2019, **58**, 99.
12 K. Nomiya, Y. Kondoh, K. Onoue, N. C. Kasuga, H. Nagano, M. Oda, T. Sudoh and S. Sakuma, *J. Inorg. Biochem.*, 1995, **58**, 255.
13 (*a*) L. G. AbdulHalim, N. Kothalawala, L. Sinatra, A. Dass and O. M. Bakr, *J. Am. Chem. Soc.*, 2014, **136**, 15865; (*b*) L. Tang, X. Kang, X. Wang, X. Zhang, X. Yuan and S. Wang, *Inorg. Chem.*, 2021, **60**, 3037.
14 G. Moreno-Alcántar, G. Romo-Islas, M. Flores-Álamo and H. Torrens, *Inorg. Chem. Commun.*, 2018, **95**, 149.
15 (*a*) X.-Y. Li, Z. Wang, H.-F. Su, S. Feng, M. Kurmoo, C.-H. Tung, D. Sun and L.-S. Zheng, *Nanoscale*, 2017, **9**, 3601; (*b*) J.-L. Jin, Y.-L. Shen, L.-W. Mi, Y.-P. Xie and X. Lu, *Chin. J. Struct. Chem.*, 2022, **41**, 2203100.
16 G. R. Desiraju and R. Parthasarathy, *J. Am. Chem. Soc.*, 1989, **111**, 8725.
17 I. Y. Chernyshov, I. V. Ananyev and E. A. Pidko, *Chem. Phys. Chem.*, 2020, **21**, 370.
18 S. K. Kurtz and T. T. Perry, *J. Appl. Phys.*, 1968, **39**, 3798.
19 (*a*) L. Cheng, L. Zhang, Q. Cao, S. Gou, X. Zhang and L. Fang, *CrystEngComm*, 2012, **14**, 7502; (*b*) C. Gao, J. Zhou, M. Cui, D. Chen, L. Zhou, F. Li and X.-L. Li, *Inorg. Chem. Front.*, 2022, **9**, 284.
20 D. H. Whiffen, *J. Chem. Soc.*, 1956, 1350.
21 P. Sun, M. Xie, L.-M. Zhang, J.-X. Liu, J. Wu, D.-S. Li, S.-F. Yuan, T. Wu and D. Li, *Angew. Chem., Int. Ed.*, 2022, **61**, e202209971.
22 O. Veselska, L. Cai, D. Podbevšek, G. Ledoux, N. Guillou, G. Pilet, A. Fateeva and A. Demessence, *Inorg. Chem.*, 2018, **57**, 2736.
23 L. Okhrimenko, C. Cibaka Ndaya, A. Fateeva, G. Ledoux and A. Demessence, *New J. Chem.*, 2020, **44**, 17970.

 